International Journal of Engineering Trends and Technology
ISSN: 2231–5381 / https://doi.org/10.14445/22315381/IJETT-V73I8P118

Volume 73 Issue 8, 214-224, August 2025

Original Article

Multicollinearity Jaccard Indexive Optimized Tuning Deep Belief Network Classification for Ulcer Recognition

S. Bhuvaneswari[1], M. Sulthan Ibrahim[2]

[1]*Department of Computer Application, Madurai Kamaraj University, Madurai, Tamil Nadu, India.*
[2]*Department of Computer Science, Govt Arts and Science College, Veerapandi, Theni, Tamil Nadu, India.*

[1]*Corresponding Author : bhuvaneswari28191@gmail.com*

Received: 04 April 2025 Revised: 30 July 2025 Accepted: 12 August 2025 Published: 30 August 2025

Abstract - *An ulcer refers to a painful sore in the lining of the small intestine. Sometimes, ulcers indicate underlying conditions such as gastrointestinal cancers. A novel Multicollinearity Jaccard Index-Optimised Tuning Deep Belief Network (MJIOTDBN) is developed to enhance ulcer prediction accuracy by efficient classification within minimum time consumption. Initially, a dataset containing numerous Wireless Capsule Endoscopy (WCE) images was collected in the acquisition phase. A Deep Belief Network (DBN) is a fully connected artificial feed-forward deep learning method comprising two visible layers, input and output layers, and multiple hidden layers. It involves two primary steps. In the layer-by-layer process, each network layer receives weighted input, uses the Multicollinearity Jaccard Index for feature transformation, and passes outputs to subsequent layers. In fine-tuning, error backpropagation algorithms adjust hyperparameters optimally using the Nesterov Accelerated Gradient descent method to increase the accuracy of ulcer classification. This optimized fine-tuning process enhances the deep neural networks and overall learning efficiency. Contrary to DL, experimental analysis of the MJIOTDBN method improves the accuracy of classification with minimal time.*

Keywords - *Ulcer detection, WCE Images, Multicollinearity Jaccard Index, Deep Belief Network, Nesterov accelerated gradient descent method.*

1. Introduction

Ulcer disease prediction is a vital aspect of medical diagnostics, focusing on the early detection and treatment of ulcers to prevent severe complications. At ML and DL, advanced techniques significantly enhanced the ability to predict and detect ulcers early, thereby improving patient outcomes. MSSADL-GITDC was developed in [1] with the aim of achieving improved classification accuracy. It failed to classify the disease effectively within a minimal time. A multi-classification DL model called VGG19 + CNN was introduced in [2] to accurately detect ulcers.

However, achieving optimal hyperparameter tuning was a difficult task. CNN was developed in [3] for the diagnosis of intestinal diseases. A deep CNN was designed in [4] for the automatic detection of ulcers using different ratios of augmented datasets.

A deep CNN was developed in [5] to achieve a reliable and efficient approach for classifying gastrointestinal tract abnormalities using WCE images with low computational cost. A 3D-CNN was designed in [6] for automatic multiclass classification by utilizing spatiotemporal information to facilitate the WCE diagnosis process. Two deep learning networks, VGG-19 and ResNet-50, were developed in [7] for classifying gastrointestinal diseases. In [8], four deep learning models were developed for detecting bleeding peptic ulcer disease.

For automatic detection and classification, a DL-based system was developed in [9]. A novel deep semantic segmentation approach was designed in [10]. A fully automated system based on deep learning feature fusion and selection was developed for recognizing stomach infections using ulcer images. A VAE-GAN architecture was designed in [11] for ulcer identification using endoscopic images. A CNN was developed in [12] for automatic classification and diagnosis. A novel computer-aided diagnosis method was designed in [13] for detecting abnormalities using WCE images. A transfer learning approach to reuse features from pre-trained neural networks was introduced in [14] for classifying images into those with and without lesions. Table 1 shows the comparison of existing methods.

Table 1. Comparison of existing methods

Method & Reference No	Contribution	Research Findings	Demerits
MSSADL-GITDC [1]	MSSADL-GITDC was introduced to achieve the maximum accuracy of classification	MSSA helps to enhance accuracy by 98%	The disease was not classified within a minimal time
VGG19 + CNN [2]	VGG19 + CNN was developed for the accurate detection of ulcers	Vgg-19 + CNN achieved an F1-score of 98.10%	Hyperparameter tuning was not considered
CNN [3]	CNN was designed for the diagnosis of intestinal diseases	Enhanced sensitivity by 96% and specificity by 97%	Accuracy was not enhanced
Deep CNN [4]	Deep CNN was discussed for the automatic detection of ulcers	Higher prediction accuracy by 96%	Ulcer diagnosis efficiency was not enhanced
Deep CNN [5]	A deep CNN was analyzed to classify gastrointestinal tract abnormalities	Improved precision by 98.9%	Failed to incorporate additional trained architectures
3D-CNN [6]	3D-CNN was investigated for automatic multiclass classification	Sensitivity is increased by 98.92%	Computational time was improved
Two deep learning networks VGG-19 and ResNet-50 [7]	Two deep learning networks, VGG-19 and ResNet-50, were designed to find gastrointestinal diseases	ResNet-50 greatest accuracy of 96.81%, and VGG-19 highest accuracy of 94.21%,	Failed to utilize advanced deep learning algorithms
Deep learning models [8]	Four deep learning models were analyzed for detecting bleeding peptic ulcer disease.	Sensitivity and specificity were 94.83% and 92.36%	Failed to improve clinical decision-making
DL-based system [9]	A deep learning-based system was investigated for the automatic detection and classification of small bowel lesions.	Achieved a higher sensitivity of 92%	Failed to conduct a larger test
Deep semantic segmentation approach [10]	A deep semantic segmentation approach was developed for 3D segmentation of various types of stomach infections.	Achieved up to 90% prediction performance	The accuracy of stomach infection detection was not improved

1.1. Research Gap

Several ML and DL approaches were developed for the gastrointestinal tract using endoscopy images. However, the conventional DL method focused on limited WCE images for ulcer detection. Different hyperparameters have a vital impact on the efficiency of the DL model. Hyperparameters such as epoch count, batch size, and learning rate selection are necessary to attain an effective outcome. Also, accurate and timely detection faces major challenges. Therefore, the proposed MJIOTDBN method is introduced using endoscopy images to enhance the accuracy and reduce the time. Also, the hyperparameter is adjusted to enhance the learning efficiency.

1.2. Novelty and Contributions of the Proposed Method

- The proposed MJIOTDBN method is developed to achieve accurate ulcer detection with higher accuracy and in less time.
- A Laplace kernel linear box filter is employed in MJIOTDBN for image preprocessing to remove the noise from the image and enhance the image quality.
- Segmentation processes and feature extraction are carried out to separate and analyze the infected region using Sokal–Michener's simple matching. In this way, ulcer detection time is reduced.
- The Multicollinearity Jaccard Index is employed in MJIOTDBN to determine the similarity between extracted features. Also, the softmax function is applied to offer accurate classification results with maximum precision.
- Nesterov Accelerated Gradient descent is applied to minimize classification error.
- Experiments were conducted for MJIOTDBN using various metrics and compared to existing methods.

2. Related Works

A custom-built CNN model was designed in [15] to classify WCE images of bleeding with improved accuracy, precision, recall, and F1 score. However, validation with a larger sample size was not conducted, limiting the ability to perform further experiments. An integration of deep CNN and geometric features was introduced in [16] for detecting GI tract diseases using WCE images. However, this approach did not consider the use of a larger number of images and the computational cost of the algorithm. A deep convolutional generative adversarial network was developed in [17] for detecting GI diseases. However, it failed to improve the performance of the object detection network. A deep learning-

based hybrid stacking ensemble modeling framework was introduced in [18] for detecting and classifying GI system conditions for early diagnosis. Nevertheless, it failed to produce high performance and fast results for early diagnosis. A deep learning-based system was designed in [19] to detect lesions of various types. However, it did not achieve optimal diagnostic performance. A Random Forest-based ensemble classifier was developed in [20] to detect abnormal WCE images automatically. But it failed to address the accurate localization of abnormalities in WCE images. A new method was introduced in [21] to detect ulcer lesions using WCE images.

Nevertheless, it failed to produce a more accurate classification map with EM segmentation, affecting the segmentation score. The lightweight and efficient deep learning model developed in [22] offers robust ulcer classification. However, various contrast and illumination techniques were not explored to improve image quality. In [23], a concatenated neural network model and SVM were developed by integrating extracted features for GI disease diagnosis. However, the segmentation of the region of interest (ROI) was not considered. A non-invasive method was introduced in [24] for evaluating the small intestine and GI tract using WCE. However, it failed to improve image accuracy. A CNN-based architecture was designed in [25] to classify abnormalities in WCE video data. However, it did not reduce the complexity.

A computer-aided method was developed in [26] to detect multiple gastrointestinal (GI) diseases. In [27], an efficient GI tract disease classification method was developed to utilize an optimized brightness-controlled contrast to improve the contrast of WCE images. However, it failed to explore other hyperparameter settings-the self-supervised learning model designed in [28] for more accurate diagnosis with minimum time. CNN was developed in [29] to speed up the classification of video frames into various categories. However, it failed to extract high-level semantic features. CNN and 3D image analysis were developed in [30] to determine and segment ulcers. However, it failed to reduce the time. The DL method was designed in [31] to categorize medical images. But the computational capacity was higher. Gastric lesions were developed in [32] by using a CNN. However, the accuracy was not improved. A study investigated Artificial intelligence (AI) [33] to extract abnormal information from endoscopic images. ML and DL were introduced in [34] to discover lesions. Nevertheless, it failed to integrate hyperparameter tuning to diminish errors.

3. Proposal Methodology

Early and accurate detection of ulcers is crucial for effective clinical management, impacting patient outcomes and preventing severe complications. In this paper, MJIOTDBN is developed to accurately and timely predict the ulcer using Wireless Capsule Endoscopy Images. This technique is employed for clinical practice by enabling faster diagnosis, targeted treatment, and better preventative strategies. First, image preprocessing is carried out using a Laplace kernel linear box filter to reduce noise and enhance image quality. Secondly, the feature extraction process is carried out using Sokal–Michener's simple matching. At last, the classification is carried out using the Multicollinearity Jaccard Index to improve the accuracy and minimize the time complexity. The Nesterov accelerated gradient descent function is employed in fine-tuning for the hyperparameter model to enhance the ulcer prediction accuracy and minimize the error rate. Improving accuracy allows clinicians to initiate treatment promptly to reduce complications and enhance patient outcomes. Also, the treatment efficiency and patient safety are enhanced.

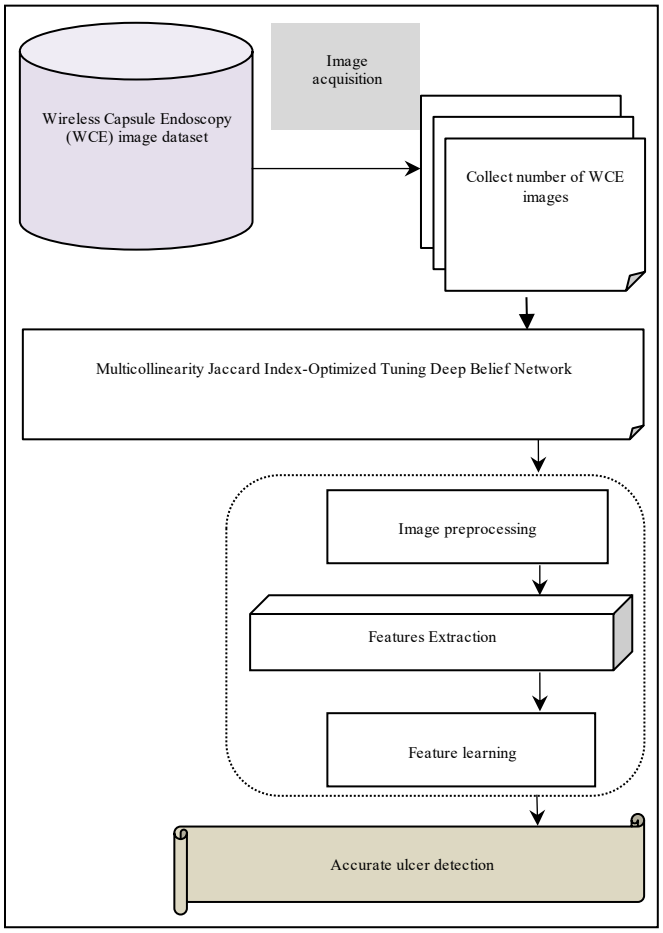

Fig. 1 Block diagram of MJIOTDBN

Figure 1 portrays the architecture diagram of the proposed MJIOTDBN technique, which includes four fundamental processes: data acquisition, preprocessing, feature extraction, and classification. DBN is an artificial neural network that is composed of multiple layers, including two visible layers, such as the input and output layers, and multiple hidden layers for processing the given input data. Two steps are involved in training a DBN: layer-by-layer and fine-tuning.

Arrangement of a deep belief network for performing multiclass classification is illustrated in Figure 2. Two steps are involved in performing multiclass classification. Layer-by-layer is an essential component in DBN, where each layer receives weighted input samples, and a set of processes is applied to transform the output to the next layer.

In fine-tuning, error backpropagation algorithms adjust hyperparameters optimally to improve the accuracy of ulcer classification. This optimized fine-tuning process enhances the classification and reduces the error rate.

In a layer-by-layer approach, a DBN employs RBMs, which are stochastic neural networks with three primary layers, such as the visible layer and the hidden layer.

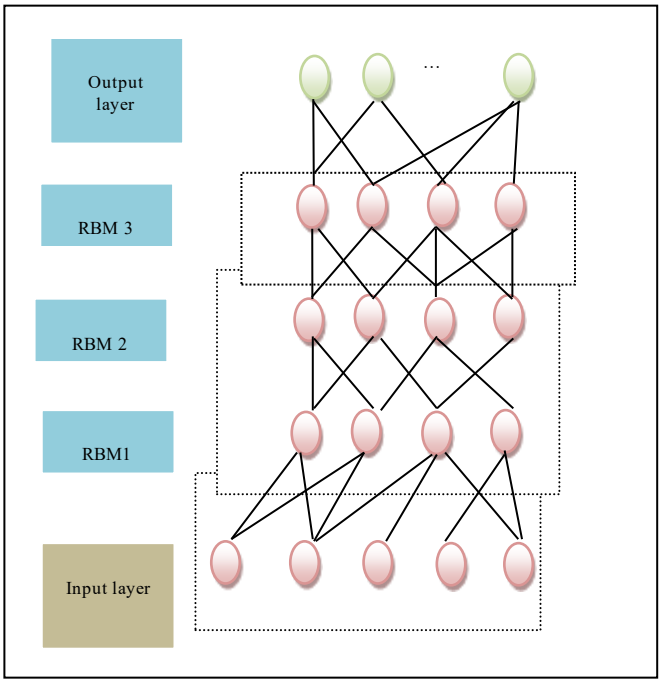

Fig. 2 Structure of DBN

Figure 2 shows that three RBM connections are employed to perform specific tasks such as preprocessing, feature extraction, and classification.

Each RBM layer is designed to handle one of these tasks. Preprocessing is performed in the first hidden layer of RBM to enhance the quality of the input image.

The hidden layer of the second RBM focuses on extracting relevant features from the preprocessed images. The hidden layer of the third RBM is used for classification, combining the features extracted by the previous RBM to accurately classify the images into predefined classes.

Each RBM layer's output serves as the input for the next layer, creating a hierarchical structure that enables the network to perform these different tasks efficiently.

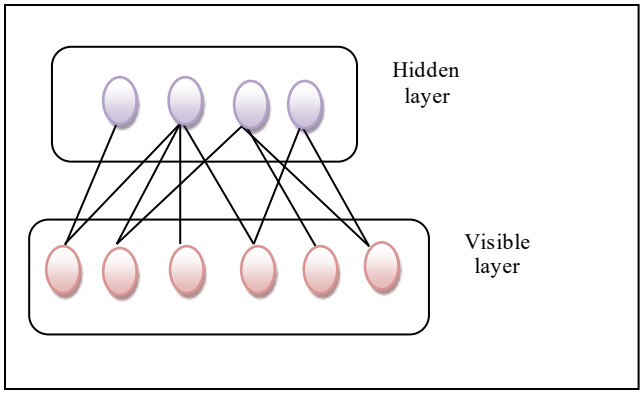

Fig. 3 Network structure of RBM

The network structure of RBM is displayed in Figure 3. This structure ensures that the network only has connections between the visible and hidden layers. The input images WCE image $EI_1, EI_2, EI_3, \ldots . EI_n$ are given to the input visible layer. At the input layer, a neuron linked by a weight '$w_1, w_2, \ldots, w_n$' as well as added bias 'B'. Measure neuron activation probability of the input visible layer 'P' as Equation (1),

$$P = \beta \left(\sum_{i=1}^{n} EI_i * w_i\right) + B \quad (1)$$

Where the sigmoid function is β, 'EI' denotes an input image, w_i Weights in the visible layer, B denote a bias of the visible layer. If the neuron activation probability is met, then the input image is transferred from the input layer into the hidden layer. In the hidden layer, the probability of a neuron in the hidden layer is measured at Equation (2),

$$P_H = \beta \left(\sum_{i=1}^{n} EI_i * w_{ih}\right) + B \quad (2)$$

Where, P_H Indicates a neuron activation probability of the hidden layer, β denotes a sigmoid activation function, 'w_{ih} denotes a weight between the visible layer and the hidden layer, B denotes a bias of the hidden layer. If neuron activation probability $P_H = 1$, then the input is transferred into the next layer. In the hidden layer, image preprocessing is an essential step for medical image analysis, which improves the quality and relevance of the image. Effective preprocessing enhances the accuracy and robustness of disease detection. The MJIOTDBN model utilizes a Laplace kernel linear box filter to enhance the image quality by removing the noise. The laplace kernel is employed for edge detection and sharpening. However, noise reduction is a challenging issue. Contrary to existing methods, linear box filters, also called mean filters, are more straightforward for blurring and noise reduction by averaging pixel values. For each image, the number of pixels p' is arranged using Equation (3) in matrix form.

$$A = \begin{bmatrix} p_{11} & p_{12} & \cdots & p_{1n} \\ p_{21} & p_{22} & \cdots & p_{2m} \\ \cdots & & & \cdots \\ p_{m1} & p_{m2} & & p_{mn} \end{bmatrix} \quad (3)$$

In Equation (3), 'A' denotes a matrix where pixels are arranged in rows and columns. The Laplace kernel is employed to find noisy pixels in the input image. It is a statistical technique employed with the kernel concept for analyzing relationships between pixels in images. The kernel analyses between pixels are given below Equation (4),

$$K = \exp\left[-\left(\frac{p_i-\mu}{D}\right)^2\right] \quad (4)$$

In Equation (4), K denotes the Laplace kernel, p_i Denotes a pixel 'μ' and 'σ' denotes the mean and standard deviation of pixels, respectively. With this, pixels that deviate from the mean are identified as noisy pixels. These noisy pixels are removed from the input image. In a linear box filter, noise at each pixel is replaced based on the average of its neighboring pixels with a filtering window (kernel). The new value of the pixel is Equation (5),

$$I_{filtered} = \frac{1}{k*k} \sum_{i=1}^{n}\sum_{j=1}^{m} p_{nn}\,(i,j) \quad (5)$$

Where, $I_{filtered}$ Denotes a filtered output, $k * k$ denotes the size of the filtering window, p_{nn} Indicates a number of pixels, i denotes a relative horizontal offset from the current pixel, j denotes a relative vertical offset from the current pixel.

As a result, quality-enhanced and smoothed images are obtained for accurate classification of the ulcers. In the second hidden layer, segment the ROI and extract significant features from the dataset. ROI segmentation in image processing isolates and analyses specific areas within an image. Sokal–Michener's simple matching is employed to extract the ROI image. The number of pixels 'p' and the similarity between neighboring pixels are estimated in Equation (6),

$$SM = 1 - \frac{|p_i \,\Delta\, p_j|}{n} \quad (6)$$

Where SM denotes a Sokal–Michener's simple matching, $p_i\, p_j$ Denotes a pixel and its neighboring pixels, n denotes the number of pixels. Based on pixel similarity, infected regions are identified from the input ROI image. The features from the input ROI image are extracted to reduce classification time. The area of a shape in an image is the number of pixels that belong to the shape using Equation (7).

$$A = \sum_{i=1}^{n}\sum_{j=1}^{m} p(i,j) \quad (7)$$

Where A denotes an area of the ROI, $p(i,j)$ is the area of all pixels within the ROI, which is measured by Equation (8) and Equation (9),

$$PR = \sum_{j=1}^{M} d_j \quad (8)$$

$$d_j = \sum_{j=1}^{M} |p_c - p_j| \quad (9)$$

Where, d_j Is the distance between the center 'p_c' is a center pixel, p_j It is a boundary pixel. The color features from the segmented ROI are extracted by transferring the RGB image into the HSV color space and identifying the distribution of color within the region. For each color channel, the mean is computed by Equation (10),

$$\mu = \frac{1}{r}\sum_{i=1}^{r} p_i \quad (10)$$

Where μ denotes a mean, μ denotes the intensity of pixels, r indicates the total number of pixels within the ROI. With the mean value, variance 'V' is estimated in Equation (11),

$$V^2 = \frac{1}{r}\sum(p_i - \mu)^2 \quad (11)$$

Where, V^2 designates the variance, p_i Indicates the intensity of a pixel, μ denotes a mean. Finally, skewness is estimated in Equation (12),

$$S = \frac{\frac{1}{r}\sum(p_i-\mu)^3}{\left(\frac{1}{r}\sum(p_i-\mu)^2\right)^{3/2}} \quad (12)$$

Where S denotes the skewness, based on the above-said mean, variance, and skewness, color features are extracted from the image. The texture provides information about the spatial display of color in a selected ROI of an image using Equation (13),

$$Tx = \frac{\sum_i \sum_j (p_i-\mu_i)(p_j-\mu_j)}{D_i\, D_j} \quad (13)$$

Where, Tx texture is a feature of an ROI image, μ_i and μ_j are means of pixels p_i, p_j, D_i and D_j Indicates a deviation of pixels. The feature vector is estimated in Equation (14),

$$FV = \{Shape, Color, Texture\} \quad (14)$$

Where FV denotes a feature vector, the extracted features are transferred into the third hidden layer using the Multicollinearity Jaccard Index for feature learning and passing outputs to subsequent layers. The Jaccard Index is measured to determine the similarity between extracted features and ground truth features. Contrary to the Jaccard Index, the Multicollinearity Jaccard Index is employed to extract the highly relevant features and remove other features. Multicol linearity indicates when two or more features are involved in the feature learning process.

The Jaccard Index ranges from 0 to 1. If the correlation coefficient provides a value of '+1', it indicates that the two features are highly correlated (multicollinearity) and '0' indicates the two features are not correlated. In this way, the Multicollinearity Jaccard Index is employed to examine the feature vector and offer multiple classification outcomes. It is mathematically expressed by Equation (15),

$$JC = \frac{FV \cap GFV}{\sum FV + \sum GFV - FV \cap GFV} \quad (15)$$

Where, JC indicates a Jaccard Similarity coefficient, FV denotes an extracted feature vector that includes shape, color and texture, GFV indicates a cluster centroid, '$\cap$' is mutual independence between data and cluster centroid, $\sum FV$ Is the sum of FV score, $\sum GFV$ Is the sum of GFV score. It provides output values from 0 to 1 $[0 \leq JC \leq 1]$.

The output of the coefficient results is given by the softmax function in Equation (16) to provide final classification results.

$$Y = \beta_{sof}(h_3 * w_{ho} \quad (16)$$

Where Y denotes an output of classification, β_{sof} denotes a softamx activation function, the prior hidden layer result is h_3, weight among hidden, w_{ho} denotes a weight between the hidden and output layer.

$$\beta_{sof} = \frac{e^{(JC)}}{\sum e^{(JC)}} \quad (17)$$

The softmax function is used in Equation (17) for multiclass classification. It calculates the probability of each class by taking the exponential of the class's coefficient ($e^{(JC)}$) and dividing it by the summation of exponentials of all class coefficients ($\sum e^{(JC)}$). Squared disparity among actual Y_{Act} as well as output classification outcomes Y_{pre} Used to estimate error rate ER in Equation (18).

$$ER = \left(Y_{Act} - Y_{pre}\right)^2 \quad (18)$$

During fine-tuning, error backpropagation algorithms such as stochastic gradient descent and Nesterov Accelerated Gradient were employed in a neural network to adjust hyperparameters optimally to increase the accuracy of ulcer classification. Backpropagation measures how to adjust weights to minimize the error between predicted and actual outputs. Nesterov Accelerated Gradient descent method is a more advanced optimization method utilized for enhancing the model performance to accelerate the learning process and improve convergence over gradient decent. Nesterov Accelerated Gradient descent method is employed in Equation (19) and Equation (20) for updating the weights. w_{t+1} .

$$w_{t+1} = w_t - \eta\ \alpha_t \quad (19)$$

$$\alpha_t = \delta\ \alpha_{t-1} + (1 - \delta)\frac{\partial ER}{\partial w_t} \quad (20)$$

Where, w_t The present weight, η is a learning rate($\eta < 1$). Huge η allots DL for discovering quicker than lesser value, fractional imitative of 'ER' in 'w_t is '$\frac{\partial ER}{\partial w_t}$', δ default value 0.9, α_t is initialized 0. Updating procedure iterated. Classification outcomes are obtained precisely at the output layer of the DBN. It optimized fine-tuning to enhance deep neural networks and overall learning efficiency.

// Algorithm 1: Multicollinearity Jaccard indexive Optimized Tuning Deep Belief Network classification
Input: Number of WCE images $EI_1, EI_2, EI_3, \ldots., EI_n$ Output: Increase the classification accuracy
Begin 1. Collect the number of WCE images. $EI_1, EI_2, EI_3, \ldots., EI_n$ taken at the input layer 2. For each image EI 3. Formulate the neuron activation probability using (1) and (2) 4. End For 5. Preprocessing the image using (4) (5) –[hidden layer 1] 6. Extract the ROI and features FV using (6) (14) 7. For each feature vector 'FV' 8. For each ground truth feature vector 'GFV' 9. Measure the Multicollinearity Jaccard Index similarity using (15) 10. End for 11. End for 12. Apply the softmax activation function using (17) to obtain classification outcomes. 13. For each classification outcome 14. Compute the error rate 'ER' using (18) 15. Apply the adaptive Gradient method to update the weight using (19) (20) 16. End for 17. Repeat the process until you find the minimum error 18. Obtain the final classification outcomes at the output layer End

4. Experimental Settings

This section compares the proposed MJIOTDBN technique and two existing methods, MSSADL-GITDC [1], VGG19 + CNN [2], in MATLAB coding in the Hyper-Kvasir dataset.

4.1. Dataset Description

To conduct the simulation, the Hyper-Kvasir dataset is taken from https://osf.io/mh9sj/. This dataset denotes the largest publicly available collection of gastrointestinal tract images for ulcer detection. It comprises 110,079 images and 373 videos obtained during Wireless Capsule Endoscopy (WCE). The dataset is divided into four main components: labeled image data, unlabeled image data, segmented image data, and annotated video content. Ulcer wireless capsule endoscopy images are gathered from these labelled images, with a total of 851 available in the dataset. Hyper-Kvasir comprises the image labels for the labeled part of the dataset, as shown in Table 2.

Table 2. Image labels in the dataset

ID	Label	ID	Label
0	barretts	12	oesophagitis-b-d
1	bbps-0-1	13	polyp
2	bbps-2-3	14	retroflex-rectum
3	dyed-lifted-polyps	15	retroflex-stomach
4	dyed-resection-margins	16	short-segment-barretts
5	hemorrhoids	17	ulcerative-colitis-0-1
6	ileum	18	ulcerative-colitis-1-2
7	impacted-stool	19	ulcerative-colitis-2-3
8	normal-cecum	20	ulcerative-colitis-grade-1
9	normal-pylorus	21	ulcerative-colitis-grade-2
10	normal-z-line	22	ulcerative-colitis-grade-3
11	oesophagitis-a		

5. Performance Results and Discussion

This section provides a comparative analysis of the MJIOTDBN technique, with two baseline (existing) methods, MSSADL-GITDC [1] and VGG19 + CNN [2]. The performance evaluation uses metrics such as ulcer detection accuracy, precision, recall, F1-score, and ulcer detection time. The performance of each MJIOTDBN technique with respect to these metrics is illustrated through tables and graphical representations. Ulcer detection accuracy refers to the ratio of the number of WCE images correctly classified as ulcers to the total number of input images. It is mathematically computed in Equation (21) as,

$$UDA = \left(\frac{TR_p+TR_n}{TR_p+TR_n+FL_p+FL_n}\right) * 100 \quad (21)$$

Where, UDA indicates ulcer detection accuracy, TR_p denotes the true positives, TR_n denoted a true negative, FL_p Denotes a false positive reference, FL_n Indicates a false negative. The accuracy is measured in percentage (%). Precision refers to the ratio of ulcer images properly recognized by the classifier. It is mathematically computed in Equation (22) as,

$$Pre = \frac{TR_p}{TR_p+FL_p} * 100 \quad (22)$$

Where, Pre is a precision, TR_p denotes a true positive, $FL_p It$ is a false positive reference.

Recall refers to the proportion of TP of actual ulcer images suitably discovered in Equation (23).

$$Rcl = \frac{TR_p}{TR_p+FL_n} * 100 \quad (23)$$

Where, Rcl denotes a recall, TR_p denotes a true positive, FL_n Indicates a false negative.

F1 score: it measures both Pre as well as Rcl using Equation (24).

$$F1\_S = 2 * \left(\frac{Pre*Rcl}{Pre+Rcl}\right) \quad (24)$$

Where $F1\_S$ denotes an F1 score, Pre denotes a precision, Rcl indicates a recall.

Ulcer detection time: The overall time for ulcer detection from the given input WCE images is measured by the algorithm's duration to identify the ulcers. It is calculated in Equation (25) as,

$$UDT = \sum_{i=1}^{n} EI_i * Tme\ [UD] \quad (25)$$

Where, UDT indicates the ulcer detection time, Tme $[UD]$ indicates a time for detection of a single image. EI_i'. It is measured in milliseconds (ms).

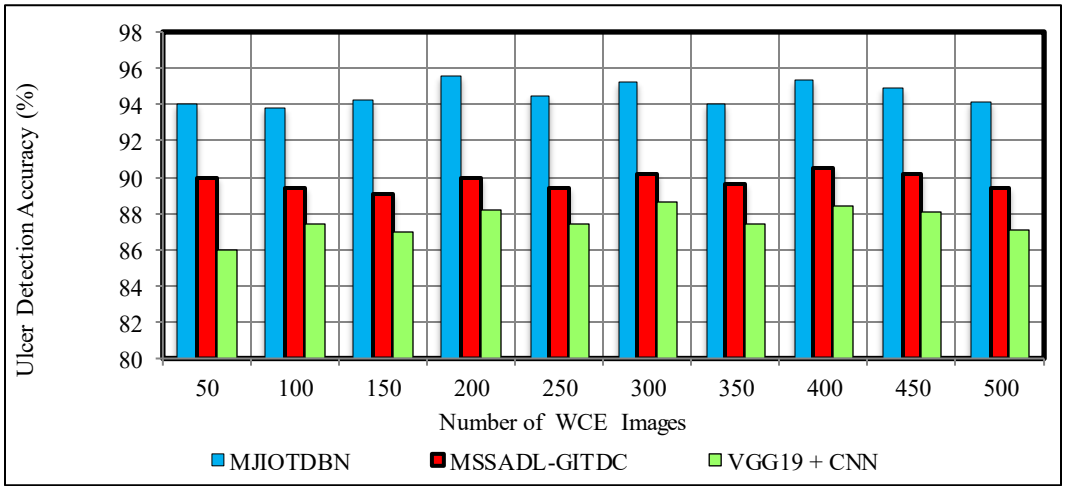

Fig. 4 Performance analysis of ulcer detection accuracy

Table 3. Comparison of precision

Number of WCE images	Precision (%)		
	MJIOTDBN	MSSADL-GITDC	VGG19 + CNN
50	94.87	92.30	89.74
100	94.55	91.05	90.65
150	95.06	90.45	88.05
200	94.33	91.22	89.45
250	95.66	92.05	90.33
300	94.05	92.33	90.04
350	95.74	90.45	88.01
400	94.33	91.2	89.33
450	95.55	92.05	90.05
500	95.2	92.33	90.12

Figure 4 depicts the ulcer detection accuracy. In Figure 4, accuracy improved by 5% and 8% for [1, 2]. Among the three methods, the MJIOTDBN technique shows especially improved accuracy performance compared to the existing methods. This improvement is due to the Multicollinearity Jaccard Index-Optimized Tuning Deep Belief Network. The extracted features and testing ground truth features are analyzed by applying a Multicollinearity Jaccard Index. The softmax activation function analyzes the similarity value and provides the classification results.

Figure 5 illustrates the precision. Precision improved in Table 3 up to 4% as well as 6% over [1, 2]. The observed results of precision using the MJIOTDBN technique were compared with the existing deep learning techniques. This improved performance is achieved by analysing the features by utilizing the Multicollinearity Jaccard Index-Optimized Tuning Deep Belief Network. Additionally, the proposed deep learning method employs the Nesterov Accelerated Gradient descent method to update the weights, minimizing the error rate in the multiclass classification results, thereby enhancing accuracy with a better true positive rate and minimal false positive rates.

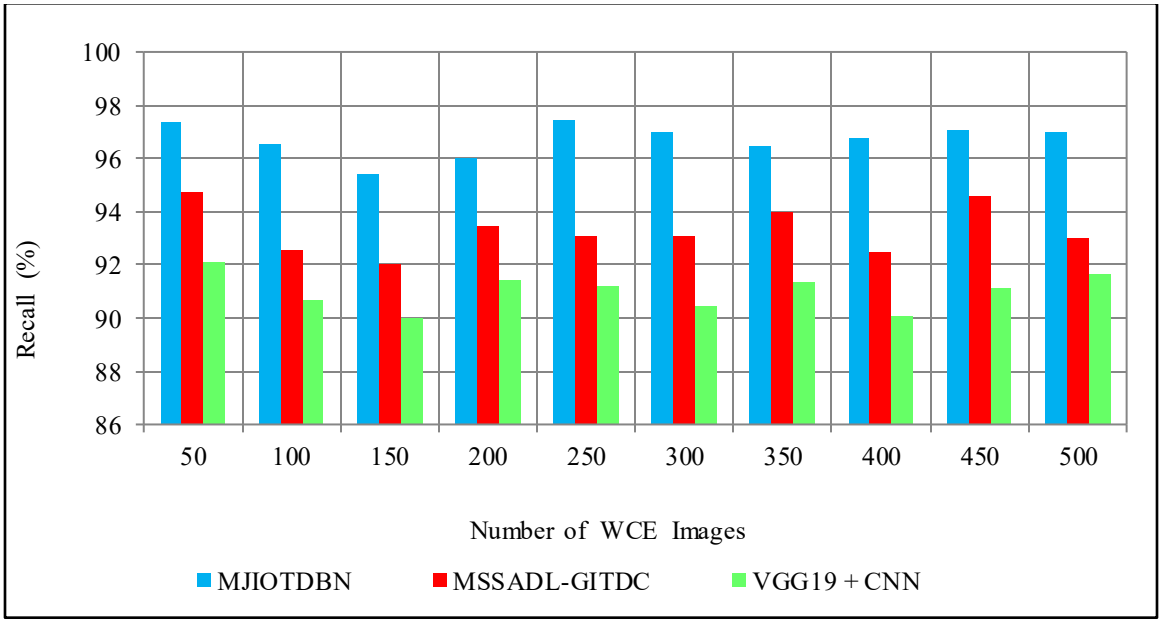

Fig. 5 performance analysis of recall

Figure 5 illustrates recall. The observed results of the MJIOTDBN technique were compared with the existing deep learning techniques. Recall accurately classifying ulcers is enhanced by 4% compared to [1] and 6% compared to [2] by applying the MJIOTDBN technique.

This improved performance is achieved by analysing the features by utilizing the Multicollinearity Jaccard Index-Optimized Tuning Deep Belief Network. Additionally, the proposed deep learning method employs the Nesterov Accelerated Gradient descent method to update the weights, minimizing the error rate in the multiclass classification results, thereby enhancing accuracy with a better true positive rate and minimal false positive rates.

Table 4. Comparison of F1-score

Number of WCE images	F1 score (%)		
	MJIOTDBN	MSSADL-GITDC	VGG19 + CNN
50	96.09	93.49	90.90
100	95.54	91.79	90.65
150	95.25	91.24	89.02
200	95.18	92.32	90.43
250	96.54	92.58	90.77
300	95.50	92.69	90.24
350	96.09	92.20	89.63
400	95.53	91.8	89.68
450	96.29	93.28	90.58
500	96.08	92.68	90.87

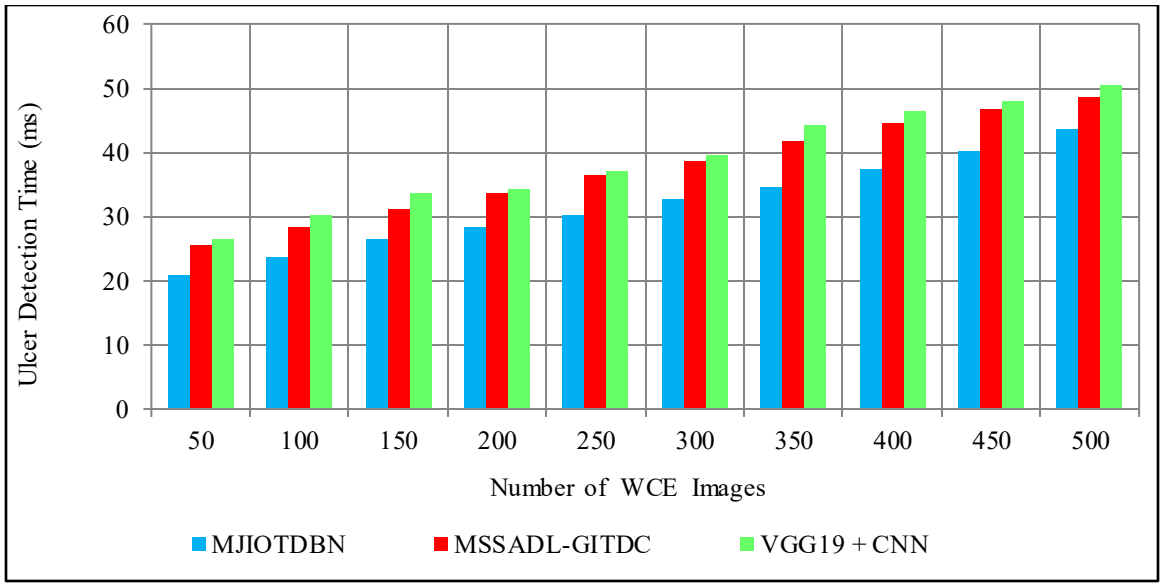

Fig. 6 Performance analysis of ulcer detection time

Table 4 describes the F1-score. It increased by 4%, 6% more than [1, 2] respectively. This indicates that the MJIOTDBN technique outperformed the existing methods in terms of achieving a higher F1-score in ulcer classification. Finally, the average of ten comparisons shows that the F1-score using the MJIOTDBN technique improved by approximately 4% and 6% compared to [1, 2], respectively.

Figure 6 demonstrates ulcer detection time. In Figure 6, the ulcer detection time minimized by 15% and 19% compared to [1, 2]. However, the MJIOTDBN technique minimizes ulcer detection time compared to existing deep learning techniques. This improvement is achieved due to the application of image preprocessing, automatic ROI segmentation, and feature extraction. The MJIOTDBN technique aims to perform accurate ulcer detection, thereby minimizing the time consumption.

6. Conclusion

With the accurate discovery of multiple classes of ulcers, the MJIOTDBN technique was introduced. The results demonstrate that the proposed MJIOTDBN technique improves accuracy, precision, recall, and F1 score, while reducing ulcer detection time compared to conventional deep learning methods. In future work, the proposed technique is extended to apply a novel deep vision transformer model to enhance the overall learning efficiency in ulcer classification tasks. Also, several metrics such as specificity and error rate are employed to measure the performance evaluation.

Data Availability Statement

The Hyper-Kvasir dataset is available within the article. The data have been gathered from (https://osf.io/mh9sj/).

References

[1] Marwa Obayya et al., "Modified Salp Swarm Algorithm with Deep Learning Based Gastrointestinal Tract Disease Classification on Endoscopic Images," *IEEE Access*, vol. 11, pp. 25959-25967, 2023. [CrossRef] [Google Scholar] [Publisher Link]

[2] Hassaan Malik et al., "Multi-Classification Deep Learning Models for Detection of Ulcerative Colitis, Polyps, and Dyed-Lifted Polyps Using Wireless Capsule Endoscopy Images," *Complex & Intelligent Systems*, vol. 10, no. 2, pp. 2477-2497, 2023. [CrossRef] [Google Scholar] [Publisher Link]

[3] Kaiwen Qin et al., "Convolution Neural Network for the Diagnosis of Wireless Capsule Endoscopy: A Systematic Review and Meta-Analysis," *Surgical Endoscopy*, vol. 36, no. 1, pp. 16-31, 2021. [CrossRef] [Google Scholar] [Publisher Link]

[4] V. Vani, and K.V. Mahendra Prashanth, "Ulcer Detection in Wireless Capsule Endoscopy Images Using Deep CNN," *Journal of King Saud University - Computer and Information Sciences*, vol. 34, no. 6, pp. 3319-3331, 2022. [CrossRef] [Google Scholar] [Publisher Link]

[5] Saqib Mahmood et al., "A Robust Deep Model for Classification of Peptic Ulcer and Other Digestive Tract Disorders Using Endoscopic Images," *Biomedicines*, vol. 10, no. 9, pp. 1-26, 2022. [CrossRef] [Google Scholar] [Publisher Link]

[6] Mehrdokht Bordbar et al., "Wireless Capsule Endoscopy Multiclass Classification Using Three-Dimensional Deep Convolutional Neural Network Model," *BioMedical Engineering OnLine*, vol. 22, no. 1, pp. 1-23, 2023. [CrossRef] [Google Scholar] [Publisher Link]

[7] Kathiresh Murugesan et al., "Homomorphic Encryption, Privacy-Preserving Feature Extraction, and Decentralized Architecture for Enhancing Privacy in Voice Authentication," *International Journal of Electrical and Computer Engineering (IJECE)*, vol. 15, no. 2, pp. 2150-2160, 2025. [CrossRef] [Google Scholar] [Publisher Link]

[8] Hsu-Heng Yen et al., "Performance Comparison of the Deep Learning and the Human Endoscopist for Bleeding Peptic Ulcer Disease," *Journal of Medical and Biological Engineering*, vol. 41, no. 4, pp. 504-513, 2021. [CrossRef] [Google Scholar] [Publisher Link]

[9] Yijie Zhu et al., "A Newly Developed Deep Learning-Based System for Automatic Detection and Classification of Small Bowel Lesions During Double-Balloon Enteroscopy Examination," *BMC Gastroenterology*, vol. 24, no. 1, pp. 1-9, 2024. [CrossRef] [Google Scholar] [Publisher Link]

[10] Javaria Amin et al., "3D-Semantic Segmentation and Classifcation of Stomach Infections Using Uncertainty Aware Deep Neural Networks," *Complex & Intelligent Systems*, vol. 8, no. 4, pp. 3041-3057, 2022. [CrossRef] [Google Scholar] [Publisher Link]

[11] Deepak Bajhaiya, Sujatha Narayanan Unni, A.K. Koushik, DM, "Deep Learning-Powered Generation of Artificial Endoscopic Images of GI Tract Ulcers," *IGIE*, vol. 2, no. 4, pp. 452-463, 2023. [CrossRef] [Google Scholar] [Publisher Link]

[12] Yixin Liu et al., "An Xception Model Based on Residual Attention Mechanism for the Classification of Benign and Malignant Gastric Ulcers," *Scientific Reports*, vol. 12, no. 1, pp. 1-12, 2022. [CrossRef] [Google Scholar] [Publisher Link]

[13] Ayoub Ellahyani et al., "Detection of Abnormalities in Wireless Capsule Endoscopy Based on Extreme Learning Machine," *Signal, Image and Video Processing*, vol. 15, no. 5, pp. 877-884, 2021. [CrossRef] [Google Scholar] [Publisher Link]

[14] Andrea Caroppoa, Pietro Sicilianoa, and Alessandro Leone, "An Expert System for Lesion Detection in Wireless Capsule Endoscopy Using Transfer Learning," Procedia Computer Science, vol. 219, pp. 1136-1144, 2023. [CrossRef] [Google Scholar] [Publisher Link]

[15] Furqan Rustam et al., "Wireless Capsule Endoscopy Bleeding Images Classification Using CNN Based Model," *IEEE Access*, vol. 9, pp. 33675-33688, 2021. [CrossRef] [Google Scholar] [Publisher Link]

[16] Ramaraj Muniappan et al., "Optimization Techniques Applied on Image Segmentation Process by Prediction of Data Using Data Mining Techniques," *International Journal of Electrical and Computer Engineering (IJECE)*, vol. 15, no. 2, pp. 2161-2171, 2025. [CrossRef] [Google Scholar] [Publisher Link]

[17] Zhiguo Xiao et al., "WCE-DCGAN: A Data Augmentation Method Based on Wireless Capsule Endoscopy Images for Gastrointestinal Disease Detection," *IET Image Processing*, vol. 17, no. 4, pp. 1170-1180, 2023. [CrossRef] [Google Scholar] [Publisher Link]

[18] Esra Sivari et al., "A New Approach for Gastrointestinal Tract Findings Detection and Classification: Deep Learning-Based Hybrid Stacking Ensemble Models," *Diagnostics*, vol. 13, no. 4, pp. 1-22, 2023. [CrossRef] [Google Scholar] [Publisher Link]

[19] Hiroaki Saito et al., "Automatic Detection and Classification of Protruding Lesions in Wireless Capsule Endoscopy Images Based on a Deep Convolutional Neural Network," *Gastrointestinal Endoscopy*, vol. 92, no. 1, pp. 144-151, 2020. [CrossRef] [Google Scholar] [Publisher Link]

[20] Velumani Thiyagarajan et al., "Adaptive Feature Learning for Robust Pathogen Detection in Plants," *2024 4th International Conference on Sustainable Expert Systems (ICSES)*, Kaski, Nepal, pp. 1347-1353, 2024. [CrossRef] [Google Scholar] [Publisher Link]

[21] Zahra Amiri, Hamid Hassanpour, and Azeddine Beghdadi, "Abnormalities Detection in Wireless Capsule Endoscopy Images Using EM Algorithm," *The Visual Computer*, vol. 39, no. 7, pp. 2999-3010, 2022. [CrossRef] [Google Scholar] [Publisher Link]

[22] Mousa Alhajlah, "Robust Ulcer Classification: Contrast and Illumination Invariant Approach," *Diagnostics*, vol. 12, no. 12, pp. 1-13, 2022. [CrossRef] [Google Scholar] [Publisher Link]

[23] Melaku Bitew Haile et al., "Detection and Classification of Gastrointestinal Disease Using Convolutional Neural Network and SVM," *Cogent Engineering*, vol. 9, no. 1, pp. 1-23, 2022. [CrossRef] [Google Scholar] [Publisher Link]

[24] Velumani Thiyagarajan et al., "Comprehensive Analysis of Cognitive Radio Technologies and its Applications," *International Conference on Soft Computing and Signal Processing*, Hyderabad, India, vol. 2, pp. 103-115, 2024. [CrossRef] [Google Scholar] [Publisher Link]

[25] Md. Jahin Alam et al., "RAt-CapsNet: A Deep Learning Network Utilizing Attention and Regional Information for Abnormality Detection in Wireless Capsule Endoscopy," *IEEE Journal of Translational Engineering in Health and Medicine*, vol. 10, pp. 1-8, 2022. [CrossRef] [Google Scholar] [Publisher Link]

[26] Amit Kumar Kundu, Shaikh Anowarul Fattah, and Khan A. Wahid, "Multiple Linear Discriminant Models for Extracting Salient Characteristic Patterns in Capsule Endoscopy Images for Multi-Disease Detection," *IEEE Journal of Translational Engineering in Health and Medicine*, vol. 8, pp. 1-11, 2020. [CrossRef] [Google Scholar] [Publisher Link]

[27] Muhammad Nouman Noor et al., "Efficient Gastrointestinal Disease Classification Using Pretrained Deep Convolutional Neural Network," *Electronics*, vol. 12, no. 7, pp. 1-20, 2023. [CrossRef] [Google Scholar] [Publisher Link]

[28] Guillem Pascual et al., "Time-Based Self-Supervised Learning for Wireless Capsule Endoscopy," Computers in Biology and Medicine, vol. 146, pp. 1-10, 2022. [CrossRef] [Google Scholar] [Publisher Link]

[29] Parminder Kaur, and Rakesh Kumar, "Performance Analysis of Convolutional Neural Network Architectures Over Wireless Capsule Endoscopy Dataset," *Bulletin of Electrical Engineering and Informatics*, vol. 13, no. 1, pp. 312-319, 2024. [CrossRef] [Google Scholar] [Publisher Link]

[30] Rosanna Cavazzana et al., "Enhancing Clinical Assessment of Skin Ulcers with Automated and Objective Convolutional Neural Network-Based Segmentation and 3D Analysis," *Applied Science*, vol. 15, no. 2, pp. 1-18, 2025. [CrossRef] [Google Scholar] [Publisher Link]

[31] Junaid Aftab et al., "Artificial Intelligence Based Classification and Prediction of Medical Imaging Using a Novel Framework of Inverted and Self-Attention Deep Neural Network Architecture," *Scientific Reports*, vol. 15, no. 1, pp. 1-16, 2025. [CrossRef] [Google Scholar] [Publisher Link]

[32] Byeong Soo Kim et al., "Enhanced Multi-Class Pathology Lesion Detection in Gastric Neoplasms Using Deep Learning-Based Approach and Validation," *Scientific Reports*, vol. 14, no. 1, pp. 1-9, 2024. [CrossRef] [Google Scholar] [Publisher Link]

[33] 1 "Artificial Intelligence-Assisted Diagnosis of Early Gastric Cancer: Present Practice and Future Prospects," *Analysis of Medicine*, vol. 57, no. 1, pp. 1-13, 2025. [CrossRef] [Google Scholar] [Publisher Link]

[34] Malinda Vania et al., "Recent Advances in Applying Machine Learning and Deep Learning to Detect Upper Gastrointestinal Tract Lesions," *IEEE Access*, vol. 11, pp. 66544-66567, 2023. [CrossRef] [Google Scholar] [Publisher Link]